Journal of Sound and Vibration 329 (2010) 5520–5531

Contents lists available at ScienceDirect

Journal of Sound and Vibration

journal homepage: www.elsevier.com/locate/jsvi

Dynamic stability of rotating flexible disk perturbed by the reciprocating angular movement of suspension–slider system

Yong-Chen Pei *, Qing-Chang Tan, Fu-Sheng Zheng, Yong-Qi Zhang

Institute of Mechanical Science and Engineering, Jilin University, Nanling Campus, Changchun, 130025, PR China

ARTICLE INFO

Article history:
Received 6 August 2009
Received in revised form
26 June 2010
Accepted 23 July 2010
Handling Editor: M.P. Cartmell
Available online 23 August 2010

ABSTRACT

To simulate the dynamic process of a magnetic head reading/writing data in a hard disk drive, a rotating flexible thin disk perturbed by the reciprocating angular movement of a suspension–slider system is modelled, where the suspension–slider system is considered as a mass–damping–spring loading system. A system dynamic model is formulated as a parametrically excited system, and its dynamic stability is studied by Hill's method involving harmonic balance. The reciprocating angular movement of the suspension–slider system causes system parametric instability at some angular movement frequencies. The large-amplitude angular movement is especially dangerous, and angular movement frequency must be reduced when the slider works at large radii of the disk. The parametric instability can be avoided or suppressed by operating at: low-frequency and small-amplitude reciprocating angular movement, small mass, large natural frequency and damping of the suspension–slider system, and low-speed rotation of the disk.

1. Introduction

Rotating disks are widely used components in mechanical engineering, such as circular saw blades, car brake disks, DVD and Blu-ray disk, and computer hard disk drives. Hence the dynamics of rotating disk systems is a subject of great interest in engineering.

Theoretically, most applications of the rotating disk can be modelled as the disk/slider problem. For computer hard disk drives, Iwan and Stahl [1] investigated the disk/slider problem by modelling a rotating spring–mass–dashpot loading system of exciting a stationary circular elastic disk, and found that stiffness, damping, and inertia of the loading system can result in parametric instability of the system. Shen [2] demonstrated that axisymmetric plate damping can suppress the instability of a stationary, elastic, annular disk excited by the rotating slider loading system. By considering the membrane stresses induced by disk rotation, Ono et al. [3] formulated a combined system of a rotating flexible disk and a pair of sliders (magnetic heads) and suspension systems that contact the disk at opposing points on its two sides, and investigated the effects of the slider assembly parameters on system natural frequency and instability. For a spinning disk in contact with a stationary load system, Chen and Bogy [4] predicted the effects of friction force, transverse mass, damping, and stiffness in the stationary load system and the stiffening of the disk due to the centrifugal force, which affects natural frequencies and stability of the spinning disk, and provided a theoretical understanding for previously reported observations based on numerical solutions. The effects of rigid-body tilting on natural frequencies and stability of the

* Corresponding author.
E-mail address: yongchen_pei@hotmail.com (Y.-C. Pei).

0022-460X/$ - see front matter © 2010 Elsevier Ltd. All rights reserved.
doi:10.1016/j.jsv.2010.07.020

disk/slider interface of a spinning flexible disk were studied both by analytical and numerical computation in Chen and Bogy [5]. Young and Lin [6] analysed the stability of a rotating flexible disk transversely contacting with a stationary oscillating unit that consists of two parallel combinations of springs and dampers attached above and under a mass. With a finite element model, Zeng and Bogy [7] simulated the shock response of a disk–suspension–slider air bearing systems in hard disk drives.

For car brake disks, friction-induced vibration and parametric resonance phenomena are areas of research activity that have received considerable attention [8]. Chan et al. [9] studied the effects of a purely frictional follower load rotating at constant angular speed around a stationary and annular plate at speeds remote from those of the parametric resonances. Mottershead et al. [10] investigated the parametric resonances that occur in a stationary annular disk under the action of a distributed mass–spring–damper system that rotates, with friction, around the disk at subcritical speeds, and found that the effects of the distributed mass and stiffness are almost neutral at subcritical speeds, but active in the supercritical range. Ouyang et al. [11,12] studied the parametric resonances and stick–slip vibration that occur when an elastic system consisting of two spring–dashpots, in the transverse and circumferential directions, and a common point mass rotates at constant angular speed around an annular flexible disk. The instability of forward and backward travelling waves was analysed in the transverse vibration of a stationary disk induced by the friction in a rotating mass–spring–damper system in Ouyang and Mottershead [13]. Ouyang and Mottershead [14] investigated the parametric resonances of a stationary disk excited by a rotating frictional load and influenced by a series of mass–spring–damper systems with or without friction, and employed a genetic algorithm to determine the right number of mass–spring–damper systems and their optimal positions in order to reduce and even eliminate the dynamic instability caused by rotating friction as a follower force on the disk surface. In Ouyang [15], Ouyang et al. [16,17], and Cao et al. [18], the vibration and dynamic instability of a car disk brake was modelled as a moving load problem on a stationary annular flexible disk acted upon by rotating components (pads, caliper, and mounting) using the finite element method; the numerical results were compared with squeal frequencies from experimental tests. Ouyang and Mottershead [19] investigated the instability of transverse vibration of an elastic disk excited by two corotating sliders on either side of the disk; firstly they took into account the bending couple acting in the circumferential direction produced by the different friction forces on the two sides of the disk, and demonstrated that disk vibration can be suppressed by suitable assignment of parameter values of the sliders.

The above research [1–19] on the disk/slider problem all considered that radial position of the slider loading system on the disk was constant and immovable. By simplifying the slider loading system as a transverse concentrated force, Weisensel and Schlack [20,21] investigated the dynamic response of a stationary elastic annular disk to rotating concentrated force of a harmonically time-varying amplitude with sudden and harmonic changes in radial position, respectively. With the same simplification of the slider loading system, Huang and Chiou [22] modelled a spinning flexible disk under a harmonically varying force travelling in the radial direction, and found that the force travelling speed acts as a driving frequency and causes resonances at certain speeds. In reality, the simplification in Refs [20–22] may be unreasonable in modelling the disk/slider problem in hard disk drives, because inertia, damping, and stiffness of the slider loading system can all result in system instability [1–6,8,13,19], but the transverse concentrated force cannot.

In this paper, the suspension–slider system in the hard disk drive was considered as a mass–damping–spring loading system, and a rotating flexible disk perturbed by reciprocating angular movement of the suspension–slider system was modelled to simulate the dynamic process of magnetic head reading/writing data. The system model was formulated as a parametrically excited system, and its dynamic stability was investigated by Hill's method involving harmonic balance [23].

2. Equation of motion

As shown in Fig. 1, a flexible thin disk that is clamped at inner radius b, free at outer radius a, and rotating at a constant angular speed Ω around its centre O is considered, and disk thickness h is very small compared with the outer radius.

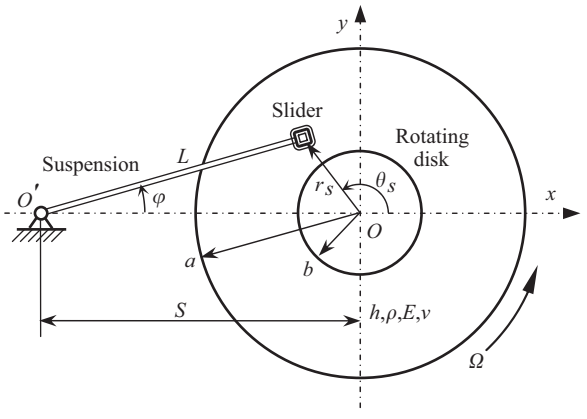

Fig. 1. Rotating flexible disk under the suspension–slider system.

The suspension rotates around its one end O' and clamps a slider at the other end. The suspension length is L and the distance O–O' is S. The suspension–slider system is modelled as a mass–damping–spring $m_s-c_s-k_s$ loading system [1,2,6] located at (r_s,θ_s) of the disk. The disk and the slider are assumed to have the same deflection at the contact point. Including a viscous damping c, the governing equation of the rotating flexible disk incorporating the slider is established in polar coordinates (r,θ) fixed on the ground as

$$\rho h\left(\frac{\partial^2 w}{\partial t^2}+2\Omega\frac{\partial^2 w}{\partial t\,\partial\theta}+\Omega^2\frac{\partial^2 w}{\partial\theta^2}\right)+c\left(\frac{\partial w}{\partial t}+\Omega\frac{\partial w}{\partial\theta}\right)+\frac{Eh^3}{12(1-\nu^2)}\nabla^4 w \quad -\rho h a^2\Omega^2\left[\frac{1}{r}\frac{\partial}{\partial r}\left(r\sigma_r\frac{\partial w}{\partial r}\right)+\frac{1}{r^2}\frac{\partial}{\partial\theta}\left(\sigma_\theta\frac{\partial w}{\partial\theta}\right)\right]$$
$$+\frac{\delta_{r,r_s}\delta_{\theta,\theta_s}}{r}(m_s\ddot{w}+c_s\dot{w}+k_s w)=0 \tag{1}$$

where $\nabla^4=\left(\partial^2/\partial r^2+(1/r)(\partial/\partial r)+(1/r^2)(\partial^2/\partial\theta^2)\right)^2$ is a bi-harmonic differential operator, E is Young's modulus, ν is Poisson's ratio, ρ is mass per unit volume of the disk, and $\delta_{\bullet,\bullet}$ is the Dirac delta function. In Eq. (1), σ_r and σ_θ are the disk membrane stress resultants expressed using the zero displacement model [6,23]:

$$\sigma_r=[8b_0(a/r)^2+8b_1-(3+\nu)(r/a)^2]/8$$
$$\sigma_\theta=[-8b_0(a/r)^2+8b_1-(1+3\nu)(r/a)^2]/8 \tag{2}$$

where

$$b_0=\frac{(1-\nu)(b/a)^2[(3+\nu)-(1+\nu)(b/a)^2]}{8[(1+\nu)+(1-\nu)(b/a)^2]}$$
$$b_1=\frac{(1+\nu)[(3+\nu)+(1-\nu)(b/a)^4]}{8[(1+\nu)+(1-\nu)(b/a)^2]}$$

At the clamped edge $r=b$, the boundary conditions of the transverse deflection are

$$w|_{r=b}=0,\quad \partial w/\partial r|_{r=b}=0 \tag{3}$$

Since the bending moment and shear force in the disk are zero at the free edge $r=a$, the boundary conditions are

$$\left[\frac{\partial^2 w}{\partial r^2}+\nu\left(\frac{1}{r}\frac{\partial w}{\partial r}+\frac{1}{r^2}\frac{\partial^2 w}{\partial\theta^2}\right)\right]\Bigg|_{r=a}=0$$
$$\left[\frac{\partial}{\partial r}\left(\frac{\partial^2 w}{\partial r^2}+\frac{1}{r}\frac{\partial w}{\partial r}+\frac{1}{r^2}\frac{\partial^2 w}{\partial\theta^2}\right)+\frac{1-\nu}{r^2}\frac{\partial^2}{\partial\theta^2}\left(\frac{\partial w}{\partial r}-\frac{w}{r}\right)\right]\Bigg|_{r=a}=0 \tag{4}$$

Using the Bessel functions as the radial shape function of the disk [1,2,6,9–14,16–19,23], the solution of Eq. (1) can be assumed to be

$$w=\sum_{m=0}^{\infty}\sum_{n=-\infty}^{\infty}\mathrm{e}^{\mathrm{i}n\theta}\boldsymbol{B}_n(\kappa_{m,n}r)\boldsymbol{c}_{m,n}x_{m,n}(t) \tag{5}$$

where m, n are the numbers of nodal circles and nodal diameters, respectively, $x_{m,-n}=\mathrm{conj}(x_{m,n})$, the operator conj(•) stands for complex conjugate, the radial shape function vector [23] $\boldsymbol{B}_n(\kappa_{m,n}r)=\left[\mathrm{J}_n(\kappa_{m,n}r)\quad \mathrm{Y}_n(\kappa_{m,n}r)\quad \mathrm{I}_n(\kappa_{m,n}r)\quad \mathrm{K}_n(\kappa_{m,n}r)\right]$, $\boldsymbol{c}_{m,n}=\left[c_1\quad c_2\quad c_3\quad c_4\right]^T$, and $\boldsymbol{B}_n(\kappa_{m,n}r)\boldsymbol{c}_{m,n}=\boldsymbol{B}_{-n}(\kappa_{m,-n}r)\boldsymbol{c}_{m,-n}$; $\kappa_{m,n}$ and $\boldsymbol{c}_{m,n}$ can be determined by the self-adjoint eigenvalue problem corresponding to Eqs. (1)–(4) for a stationary disk [1,23]. In addition, the orthonormality condition for the radial mode shape $\boldsymbol{B}_n(\kappa_{m,n}r)\boldsymbol{c}_{m,n}$ is

$$\int_b^a[\boldsymbol{B}_n(\kappa_{m_1,n}r)\boldsymbol{c}_{m_1,n}\boldsymbol{B}_n(\kappa_{m_2,n}r)\boldsymbol{c}_{m_2,n}]r\,\mathrm{d}r=\delta_{m_1,m_2} \tag{6}$$

With Galerkin's method [23], substituting Eq. (5) into Eq. (1), multiplying Eq. (1) by $\mathrm{e}^{-\mathrm{i}n\theta}\boldsymbol{B}_n(\kappa_{m,n}r)\boldsymbol{c}_{m,n}$ and integrating both sides over the disk area ($r\in[b,a]$, $\theta\in[0,2\pi]$), an ordinary differential system is obtained as

$$\ddot{\boldsymbol{x}}_n+(c/\rho/h+\mathrm{i}2n\Omega)\dot{\boldsymbol{x}}_n+(\mathbf{S}_n+\Omega^2\mathbf{L}_n-n^2\Omega^2\mathbf{I}_1+\mathrm{i}cn\Omega\mathbf{I}_1/\rho/h)\boldsymbol{x}_n+\sum_{k=-N_n}^{N_n}\frac{\mathrm{e}^{\mathrm{i}(-n+k)\theta_s}}{2\pi\rho h}\mathbf{H}_{n,k}(r_s)(m_s\ddot{\boldsymbol{x}}_k+c_s\dot{\boldsymbol{x}}_k+k_s\boldsymbol{x}_k)=\boldsymbol{0} \tag{7}$$

where $\boldsymbol{x}_n=\left[\cdots\quad x_{m,n}\quad\cdots\right]^T$ and $m=0,1,\cdots,N_m$. $\mathbf{I}_1$, $\mathbf{S}_n$, $\mathbf{L}_n$, and $\mathbf{H}_{n,k}(r_s)$ can be found in Appendix C.

Let $\boldsymbol{X}=\left[\ldots\quad \boldsymbol{x}_n{}^T\quad\ldots\right]^T$ and $n=-N_n,\ldots,-1,0,1,\ldots,N_n$. Rearranging Eq. (7) yields

$$[\mathbf{I}+m_s\mathbf{H}(r_s,\theta_s)]\ddot{\boldsymbol{X}}+[c\mathbf{I}/\rho/h+\mathrm{i}2\Omega\mathbf{I}_n+c_s\mathbf{H}(r_s,\theta_s)]\dot{\boldsymbol{X}}+[\mathbf{S}+k_s\mathbf{H}(r_s,\theta_s)+\Omega^2(\mathbf{L}-\mathbf{I}_{n^2})+\mathrm{i}c\Omega\mathbf{I}_n/\rho/h]\boldsymbol{X}=\boldsymbol{0} \tag{8}$$

See Appendix D for $\mathbf{S}$, $\mathbf{L}$, $\mathbf{I}$, $\mathbf{I}_n$, $\mathbf{I}_{n^2}$, and $\mathbf{H}(r_s,\theta_s)$.

As illustrated in Fig. 1, coordinates of the slider on disk can be solved as

$$r_s(\varphi)=\sqrt{S^2+L^2-2SL\cos(\varphi)} \tag{9}$$

$$\theta_s(\varphi)=\pi-\tan^{-1}\left(\frac{L\sin(\varphi)}{S-L\cos(\varphi)}\right) \tag{10}$$

where φ is the suspension moving angle.

The range of the suspension angular movement can be written as

$$\varphi\in[\varphi_1,\varphi_2] \tag{11}$$

where

$$\varphi_1=\cos^{-1}\left(\frac{S^2+L^2-b^2}{2SL}\right) \quad \text{and}$$
$$\varphi_2=\cos^{-1}\left(\frac{S^2+L^2-a^2}{2SL}\right)$$

It can be assumed that the suspension moves over a small range Δ around φ_0:

$$\varphi=\varphi_0+\Delta \tag{12}$$

where $\varphi_0=\varphi_1+\alpha(\varphi_2-\varphi_1)$. The dimensionless slider position α indicates the radii of disk track where the slider is positioned.

Expanding $\mathbf{H}(r_s,\theta_s)$ into a Taylor series with respect to φ around φ_0 yields

$$\mathbf{H}(r_s,\theta_s)=\mathbf{H}^0+\Delta\mathbf{H}'+\Delta^2\mathbf{H}'' \tag{13}$$

where $\mathbf{H}^0$, $\mathbf{H}'$, and $\mathbf{H}''$ are given in Appendix D.

Without loss of generality, a periodically reciprocating angular movement of the suspension–slider system is assumed:

$$\Delta=\varepsilon(p\mathrm{e}^{\mathrm{i}\omega t}+\overline{p}\mathrm{e}^{-\mathrm{i}\omega t}) \tag{14}$$

where $|p|=1/2$, $\overline{p}=\mathrm{conj}(p)$; $\varepsilon=\beta(\varphi_2-\varphi_1)$, ω and β are the frequency and dimensionless amplitude of the reciprocating angular movement, respectively, $\alpha+\beta\le 1$, and $\alpha-\beta\ge 0$. The angular movement frequency ω indicates the magnetic head read/write speed in the hard disk drive.

Substituting Eqs. (13) and (14) in Eq. (8) yields a dynamic model of the rotating flexible disk perturbed by the reciprocating angular movement of the suspension–slider system:

$$\{\mathbf{I}+m_s[\mathbf{H}^0+\varepsilon(p\mathrm{e}^{\mathrm{i}\omega t}+\overline{p}\mathrm{e}^{-\mathrm{i}\omega t})\mathbf{H}'+\varepsilon^2(p\mathrm{e}^{\mathrm{i}\omega t}+\overline{p}\mathrm{e}^{-\mathrm{i}\omega t})^2\mathbf{H}'']\}\ddot{\boldsymbol{X}}+\{c\mathbf{I}/\rho/h+\mathrm{i}2\Omega\mathbf{I}_n+c_s[\mathbf{H}^0+\varepsilon(p\mathrm{e}^{\mathrm{i}\omega t}+\overline{p}\mathrm{e}^{-\mathrm{i}\omega t})\mathbf{H}'$$
$$+\varepsilon^2(p\mathrm{e}^{\mathrm{i}\omega t}+\overline{p}\mathrm{e}^{-\mathrm{i}\omega t})^2\mathbf{H}'']\}\dot{\boldsymbol{X}}+\{\mathbf{S}+\Omega^2(\mathbf{L}-\mathbf{I}_{n^2})+\mathrm{i}c\Omega\mathbf{I}_n/\rho/h+k_s[\mathbf{H}^0+\varepsilon(p\mathrm{e}^{\mathrm{i}\omega t}+\overline{p}\mathrm{e}^{-\mathrm{i}\omega t})\mathbf{H}'+\varepsilon^2(p\mathrm{e}^{\mathrm{i}\omega t}+\overline{p}\mathrm{e}^{-\mathrm{i}\omega t})^2\mathbf{H}'']\}\boldsymbol{X}=\boldsymbol{0} \tag{15}$$

Since in Eq. (15) the coefficient matrices of $\ddot{\boldsymbol{X}}$, $\dot{\boldsymbol{X}}$, and $\boldsymbol{X}$ are time-dependent, the dynamic model is a parametrically excited system.

3. System stability

Parametric instability characterized by unbounded growth of a small disturbance can happen in a parametrically excited system; thus dynamic stability of the system is of interest in engineering. From Hill's method, Takahashi [24], Turhan [25], Turhan and Koser [26], and Turhan and Bulut [27], the solution of Eq. (15) can be expressed as a product of a characteristic component and harmonic component:

$$\boldsymbol{X}=\mathrm{e}^{\lambda t}\sum_{j=-\infty}^{\infty}\boldsymbol{a}_j\mathrm{e}^{\mathrm{i}j\omega t}\approx\mathrm{e}^{\lambda t}\sum_{j=-N_j}^{N_j}\boldsymbol{a}_j\mathrm{e}^{\mathrm{i}j\omega t} \tag{16}$$

Eq. (16) can be rewritten in matrices [23] as

$$\boldsymbol{X}=\mathrm{e}^{\lambda t}\boldsymbol{\Phi}\boldsymbol{A} \tag{17}$$

where $\boldsymbol{A}=\begin{bmatrix}\cdots & \boldsymbol{a}_j^T & \cdots\end{bmatrix}^T$ and $\boldsymbol{\Phi}=\begin{bmatrix}\cdots & \mathrm{e}^{\mathrm{i}j\omega t}\mathbf{I} & \cdots\end{bmatrix}$, $j=-N_j,\ldots,-1,0,1,\ldots,N_j$. The first and second derivatives [23] of $\boldsymbol{\Phi}$ with respect to t are expressed as

$$\dot{\boldsymbol{\Phi}}=\mathrm{i}\omega\boldsymbol{\Phi}\mathbf{J}_1, \quad \ddot{\boldsymbol{\Phi}}=-\omega^2\boldsymbol{\Phi}\mathbf{J}_2 \tag{18}$$

where $\mathbf{J}_1$ and $\mathbf{J}_2$ are given in Appendix E.

Let

$$e^{-ij\omega t}\mathbf{\Phi} = \mathbf{\Phi}\mathbf{T}_j \tag{19}$$

where $\mathbf{T}_j$ is given in Appendix E.

Substituting Eqs. (17)–(19) in Eq. (15) yields

$$\begin{gathered}\{\lambda^2(\mathbf{I}\mathbf{\Phi}+m_s\mathbf{D})+\lambda[\mathbf{I}\mathbf{\Phi}c/\rho/h+2i\Omega\mathbf{I}_n\mathbf{\Phi}+2i\omega\mathbf{I}\mathbf{\Phi}\mathbf{J}_1+\mathbf{D}(c_s\mathbf{I}_D+2i\omega m_s\mathbf{J}_1)]+\\ [\mathbf{S}\mathbf{\Phi}+\Omega^2(\mathbf{L}-\mathbf{I}_{n^2})\mathbf{\Phi}-2\omega\Omega\mathbf{I}_n\mathbf{\Phi}\mathbf{J}_1-\omega^2\mathbf{I}\mathbf{\Phi}\mathbf{J}_2+i\omega\mathbf{I}\mathbf{\Phi}\mathbf{J}_1c/\rho/h+\\ ic\Omega\mathbf{I}_n\mathbf{\Phi}/\rho/h+\mathbf{D}(k_s\mathbf{I}_D+i\omega c_s\mathbf{J}_1-\omega^2m_s\mathbf{J}_2)]\}e^{\lambda t}\boldsymbol{A}=\boldsymbol{0}\end{gathered} \tag{20}$$

where

$$\mathbf{D}=\mathbf{H}^0\mathbf{\Phi}+\varepsilon\mathbf{H}'\mathbf{\Phi}(p\mathbf{T}_1{}^T+\overline{p}\mathbf{T}_1)+\varepsilon^2\mathbf{H}''\mathbf{\Phi}(p^2\mathbf{T}_2{}^T+\overline{p}^2\mathbf{T}_2+2p\overline{p}\mathbf{I}_D)$$

Dimensionless variables are introduced using

$$\begin{gathered}\lambda=(\vartheta-\eta)\Omega_{0,0},\quad \omega=\xi\Omega_{0,0},\quad \Omega=\zeta\Omega_{0,0}\\ c/\rho/h=2\eta\Omega_{0,0},\quad c_s=2m_s\eta_s\gamma_s\Omega_{0,0}\\ k_s=m_s\gamma_s{}^2\Omega_{0,0}{}^2\end{gathered} \tag{21}$$

Applying the harmonic balance method to Eq. (20) yields the quadratic eigenvalue problem

$$(\vartheta^2\mathbf{E}_2+2\vartheta\mathbf{E}_1+\mathbf{E}_0)\boldsymbol{A}=\boldsymbol{0} \tag{22}$$

where

$$\begin{gathered}\mathbf{P}=\mathbf{Q}^0+\varepsilon\mathbf{Q}'(p\mathbf{T}_1{}^T+\overline{p}\mathbf{T}_1)+\varepsilon^2\mathbf{Q}''(p^2\mathbf{T}_2{}^T+\overline{p}^2\mathbf{T}_2+2p\overline{p}\mathbf{I}_D)\\ \mathbf{E}_2=\mathbf{I}_D+m_s\mathbf{P},\ \mathbf{E}_1=i\zeta\mathbf{I}_D^n+i\xi\mathbf{J}_1+m_s\mathbf{P}[i\xi\mathbf{J}_1+(\eta_s\gamma_s-\eta)\mathbf{I}_D]\\ \mathbf{E}_0=\mathbf{K}+\zeta^2(\mathbf{K}_\sigma-\mathbf{I}_D^{n^2})-2\xi\zeta\mathbf{I}_D^n\mathbf{J}_1-\xi^2\mathbf{J}_2-\eta^2\mathbf{I}_D+m_s\mathbf{P}[(\gamma_s{}^2+\eta^2-2\eta\eta_s\gamma_s)\mathbf{I}_D+2i\xi(\eta_s\gamma_s-\eta)\mathbf{J}_1-\xi^2\mathbf{J}_2]\end{gathered}$$

$\mathbf{I}_D$, $\mathbf{I}_D^n$, $\mathbf{I}_D^{n^2}$, $\mathbf{K}$, $\mathbf{K}_\sigma$, $\mathbf{Q}^0$, $\mathbf{Q}'$, and $\mathbf{Q}''$ are given in Appendix E. The dynamic stability can be investigated by $\mathrm{Re}\,\lambda$ ($\mathrm{Re}\,\vartheta-\eta$), and the corresponding basic solution is unstable and unbounded as $t\to\infty$ when any eigenvalue λ possesses a positive real part [23].

An instability coefficient is introduced as

$$s=\max_i(\mathrm{Re}\,\vartheta_i)-\eta \tag{23}$$

From Eq. (23), system equilibrium is unstable when $s>0$; thus increase of viscous damping η can improve the system stability. Since the practical viscous damping η is small, it can be considered [23] that the equilibrium is unstable when $s>0$, and it is stable when $s=0<\eta$.

4. Numerical results and discussion

The fundamental parameters of the suspension–slider–disk system are selected to be S=58 mm, L=55 mm, a=95/2 mm, b=35/2 mm, h=0.6 mm, E=200 GPa, ρ=7840 kg m^{-3}, and ν=0.3. Furthermore, ζ=0.5, α=0.5, β=0.05, m_s=0.01 kg, η_s=0.03, and γ_s=0.2; unless otherwise stated, these values are used as default parameters in the following analysis.

Numerical convergence of the truncation number N_m of radial expansion in Bessel functions, the truncation number N_n of circumferential expansion in trigonometric functions, and the truncation number N_j of Fourier expansion in time needs to be investigated firstly. When the radial position of the slider loading system on the disk is constant, i.e. β=0 (ε=0), Eq. (22) reduces to

$$\{\vartheta^2(\mathbf{I}+m_s\mathbf{H}^0)+2\vartheta[i\zeta\mathbf{I}_n+m_s(\eta_s\gamma_s-\eta)\mathbf{H}^0]+[\mathbf{S}/\Omega_{0,0}{}^2+\zeta^2(\mathbf{L}-\mathbf{I}_{n^2})-\eta^2\mathbf{I}+m_s(\gamma_s{}^2+\eta^2-2\eta\eta_s\gamma_s)\mathbf{H}^0]\}\boldsymbol{A}=\boldsymbol{0} \tag{24}$$

With increases of N_m and N_n, numerical convergence of the instability coefficient s, from Eqs. (24) and (23), is illustrated in Fig. 2, where the contour lines indicate the number of matrix elements $(N_m+1)^2(2N_n+1)^2$ in Eq. (24). When $N_m\geq 1$ and $N_n\geq 6$, the instability coefficient s is convergent with increase of N_m and N_n. As listed in Table 1, the instability coefficient s from Eqs. (22) and (23) is also convergent as N_j increases. Since the number of matrix elements in Eq. (22), $(N_m+1)^2(2N_n+1)^2(2N_j+1)^2$, is roughly proportional to calculation time of the quadratic eigenvalue problem, under the condition of an acceptable accuracy, a proper set of (N_m,N_n,N_j) should be as small as possible to decrease the number of calculations. From Ouyang et al. [12], Fig. 2, Turhan [25], Turhan and Koser [26], Turhan and Bulut [27], and Table 1, N_m=2, N_n=12, and N_j=3 are selected to predict the fundamental instability parameter regions in this paper.

With constant and immovable radial position of the slider loading system on the disk, the research [1–6,8,13,19] indicated that inertia m_s, damping η_s, and stiffness γ_s of the loading system can all result in system instability, which is called 'constant instability' in this paper. Nevertheless, the reciprocating angular movement of the suspension–slider system results in the parametrically excited system Eq. (15), which can induce system parametric instability, called

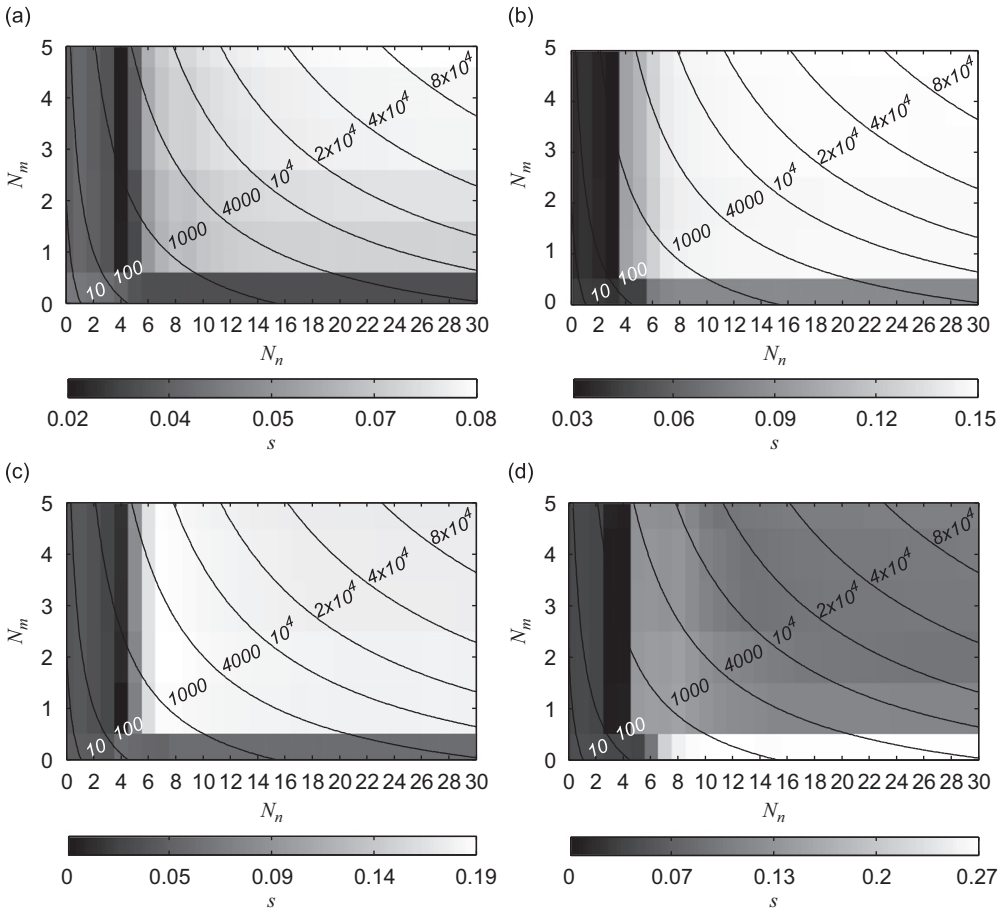

Fig. 2. Convergence of the instability coefficient with increase of truncation number N_m of radial expansion in Bessel functions and truncation number N_n of circumferential expansion in trigonometric functions. β=0. (a) ζ=1.4, (b) ζ=1.6, (c) ζ=1.8, and (d) ζ=2.0.

Table 1
Convergence of instability coefficient with increase of truncation number N_j of Fourier expansion in time. N_m=2 and N_n=12.

N_j	ξ=1.34	ξ=1.49	ξ=1.76	ξ=1.93
1	0.003530704012342	0.002350575748242	0.004720549234872	0.003465474074417
2	0.003546599849910	0.002357270651480	0.004743968093363	0.003435800926040
3	0.003546609201077	0.002357272601631	0.004744514193429	0.003435854493085
4	0.003546609203490	0.002357272600749	0.004744514437021	0.003435854427535
5	0.003546609203493	0.002357272600701	0.004744514437242	0.003435854427441
6	0.003546609203452	0.002357272600625	0.004744514437359	0.003435854427145
7	0.003546609203415	0.002357272600649	0.004744514437326	0.003435854427306
8	0.003546609203414	0.002357272600985	0.004744514437322	0.003435854426975

'reciprocating instability'. Effects of system parameters (ξ,α,β,ζ,γ_s,m_s,η_s) on the disk equilibrium stability (s) are investigated using Eqs. (22)–(23) and illustrated in grey images Figs. 3–8.

As shown in Fig. 1, slider radial position on the disk can be changed by varying the suspension moving angle φ expressed as $\varphi_1+(\varphi_2-\varphi_1)[\alpha+\beta(p\mathrm{e}^{\mathrm{i}\omega t}+\overline{p}\mathrm{e}^{-\mathrm{i}\omega t})]$ from Eqs. (12) and (14). Fig. 3 presents effects of frequency ξ and amplitude β of the reciprocating angular movement of the suspension–slider system on system stability. In the grey image, some dark parameter regions appear, where system instability occurs, since $s>0$. Specially, when β=0 (i.e. ε=0), the slider radial position is constant as presented in Refs. [1–19], the time-dependent terms vanish in Eq. (15), and the governing equation is not a parametrically excited system any more and can just induce the constant instability; thus there is no instability region in Fig. 3 for this special case. Nevertheless, some zonal dark parameter regions widen and darken with the increase of amplitude β. In other words, the reciprocating angular movement of suspension–slider system induces system instability at some angular movement frequencies ξ, and angular movement amplitude β increases the instability.

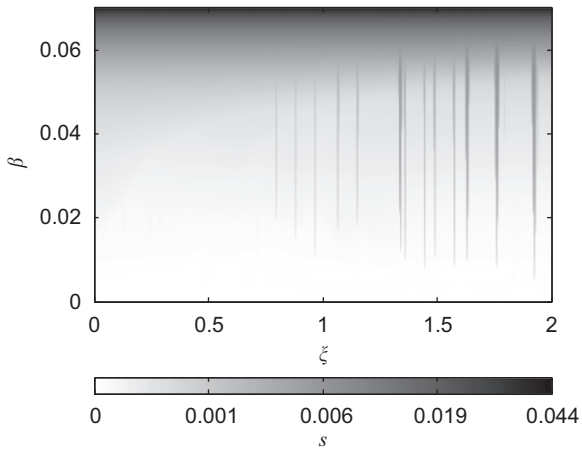

Fig. 3. Effects of reciprocating angular movement amplitude of the suspension–slider system on system stability.

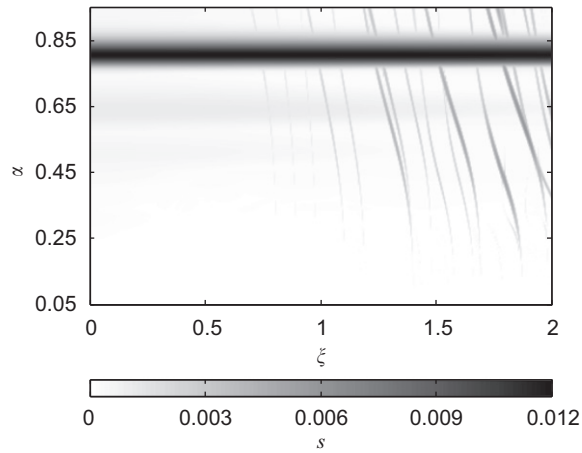

Fig. 4. Effects of slider position on system stability.

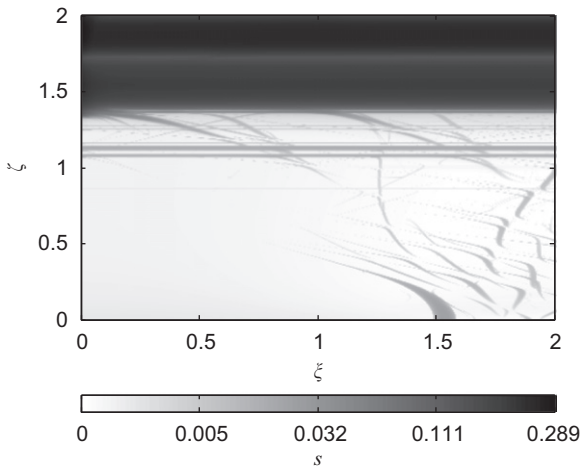

Fig. 5. Effects of disk rotating speed on system stability.

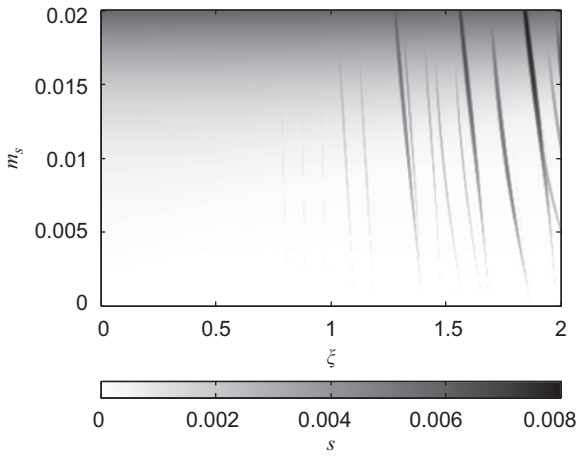

Fig. 6. Effects of mass of suspension–slider loading system on system stability.

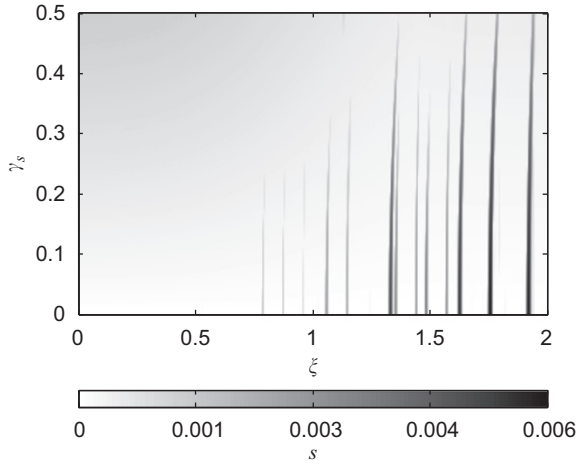

Fig. 7. Effects of natural frequency of suspension–slider loading system on system stability.

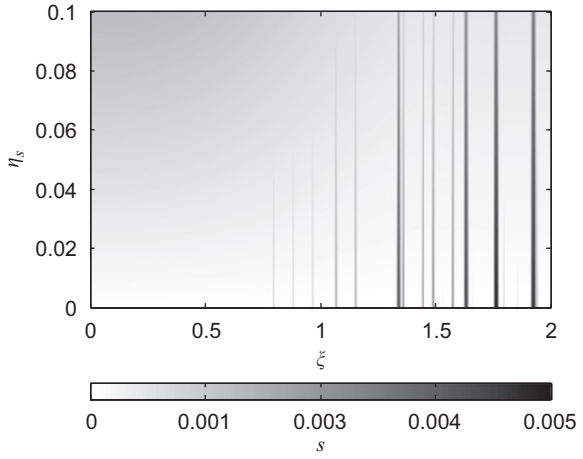

Fig. 8. Effects of damping of the suspension–slider loading system on system stability.

As shown in Fig. 3, the low-frequency and small-amplitude angular movement of the suspension–slider system is beneficial to avoid the instability. However, with further increase of amplitude β, a large instability coefficient s appears for any angular movement frequency ξ. Therefore, the large-amplitude angular movement of the suspension–slider system is especially dangerous for system stability.

The effects of slider position α on system stability are illustrated in Fig. 4. Corresponding to the constant instability, a dark parameter region parallel to the frequency axis ξ appears in Fig. 4. When the slider position α is small, the slider works on the disk inner track with small radii, and some dark zonal parameter regions implying reciprocating instability brighten due to large stiffness at small radii of the disk. As shown in Fig. 4, system instability occurs at small radii (inner track) of the disk with increase of angular movement frequency ξ. Therefore angular movement frequency of the suspension–slider system must be reduced when the slider works at large radii (outer track) of the disk.

The variations of instability parameter regions with disk rotational speed are shown in Fig. 5. There are some dark parameter regions parallel to the frequency axis ξ; these instability regions are related to the constant instability as indicated in Chen and Bogy [5] and Young and Lin [6]. However, other dark parameter regions vary with angular movement frequency ξ; that is to say they are the reciprocating instability. In the low-frequency ξ and low-speed ζ parameter region, the system equilibrium is almost stable. Since high speed is desirable to improve the performance of hard disk drives, some reasonable angular movement frequency ξ and disk speed ζ with small instability coefficient s can be selected from Fig. 5.

Fig. 6 presents the effects of mass m_s of suspension–slider loading system on system stability. When mass m_s vanishes, the suspension–slider–disk system becomes a reduced one of a single free rotating disk, and the reduced system is always stable since s=0, from Eqs. (22) and (23). With an increase of mass m_s, some dark zonal parameter regions appear in the grey image and the reciprocating instability occurs at low frequency ξ of the reciprocating angular movement. Therefore, in the design of a hard disk drive, a small-mass slider should be selected to improve system stability and increase the read/write speed. A dark region appears for large mass m_s and low frequency ξ, but the value of s in this region is very small compared with those in the zonal parameter regions.

The effects of natural frequency γ_s and damping η_s of the suspension–slider loading system on system stability are illustrated in Figs. 7 and 8, respectively. There are also some dark zonal parameter regions in the grey images. With increase of natural frequency γ_s and damping η_s, these zonal dark parameter regions for the reciprocating instability become bright and narrow. A large natural frequency γ_s results in system instability at high-frequency ξ, as shown in Fig. 7. Therefore, large natural frequency and damping of the suspension–slider loading system can be used to suppress the reciprocating instability.

5. Conclusions

In this paper, a rotating flexible disk perturbed by the reciprocating angular movement of a suspension–slider system was formulated as a parametrically excited system, and the dynamic stability of the system was investigated by Hill's method involving harmonic balance. The following conclusions on system stability can be drawn:

(1) reciprocating angular movement of the suspension–slider system induces system parametric instability at some angular movement frequencies;
(2) large-amplitude angular movement is especially dangerous, and angular movement frequency must be reduced when the slider works at large radii of the disk;
(3) the parametric instability can be avoided by operating at low-speed rotation of the disk and low-frequency, small-amplitude angular movement of the suspension–slider system;
(4) small mass and large natural frequency and damping of the suspension–slider system can be used to suppress the parametric instability.

Acknowledgments

The authors would like to thank Professor Chris Chatwin of the University of Sussex for his sincere help. This work was supported by the Fundamental Research Funds of Jilin University, PR China (Scientific Frontier and Interdisciplinary Innovation Project) under Grant no. 200903170.

Appendix A. Slider coordinates and their derivatives

$$r_0 = r_s(\varphi_0),\ r'_0 = \mathrm{d}r_s/\mathrm{d}\varphi\big|_{\varphi=\varphi_0} = SLr_0^{-1}\sin(\varphi_0)$$

$$r''_0 = \mathrm{d}^2 r_s/\mathrm{d}\varphi^2\Big|_{\varphi=\varphi_0} = SLr_0^{-1}[\cos(\varphi_0) - SLr_0^{-2}\sin^2(\varphi_0)]$$

$$\theta_0 = \theta_s(\varphi_0),$$

$$\theta'_0 = \mathrm{d}\theta_s/\mathrm{d}\varphi\big|_{\varphi=\varphi_0} = Lr_0^{-2}[L - S\cos(\varphi_0)]$$

$$\theta''_0 = \mathrm{d}^2\theta_s/\mathrm{d}\varphi^2\big|_{\varphi=\varphi_0}$$

$$= SLr_0^{-2}[(1-2L^2r_0^{-2})\sin(\varphi_0) + SLr_0^{-2}\sin(2\varphi_0)]$$

Appendix B. Derivatives of Bessel shape function vector

$$\boldsymbol{B}'_n(\kappa_{m,n}r_0)=nr_0^{-1}\boldsymbol{B}_n^{00}(\kappa_{m,n}r_0)-\kappa_{m,n}\boldsymbol{B}_n^{10}(\kappa_{m,n}r_0),\ \boldsymbol{B}''_n(\kappa_{m,n}r_0)=n(n-1)r_0^{-2}\boldsymbol{B}_n^{00}(\kappa_{m,n}r_0)+\kappa_{m,n}^2\boldsymbol{B}_n^{01}(\kappa_{m,n}r_0)+\kappa_{m,n}r_0{}^{-1}\boldsymbol{B}_n^{10}(\kappa_{m,n}r_0)$$

$$\boldsymbol{B}_n^{00}(\kappa_{m,n}r_0)=\begin{bmatrix}\mathrm{J}_n(\kappa_{m,n}r_0)\\ \mathrm{Y}_n(\kappa_{m,n}r_0)\\ \mathrm{I}_n(\kappa_{m,n}r_0)\\ \mathrm{K}_n(\kappa_{m,n}r_0)\end{bmatrix}^T,\ \boldsymbol{B}_n^{01}(\kappa_{m,n}r_0)=\begin{bmatrix}-\mathrm{J}_n(\kappa_{m,n}r_0)\\ -\mathrm{Y}_n(\kappa_{m,n}r_0)\\ \mathrm{I}_n(\kappa_{m,n}r_0)\\ \mathrm{K}_n(\kappa_{m,n}r_0)\end{bmatrix}^T$$

$$\boldsymbol{B}_n^{10}(\kappa_{m,n}r_0)=\begin{bmatrix}\mathrm{J}_{n+1}(\kappa_{m,n}r_0)\\ \mathrm{Y}_{n+1}(\kappa_{m,n}r_0)\\ -\mathrm{I}_{n+1}(\kappa_{m,n}r_0)\\ \mathrm{K}_{n+1}(\kappa_{m,n}r_0)\end{bmatrix}^T,\ \text{and}\ \boldsymbol{B}_n^{11}(\kappa_{m,n}r_0)=\begin{bmatrix}\mathrm{J}_{n+1}(\kappa_{m,n}r_0)\\ \mathrm{Y}_{n+1}(\kappa_{m,n}r_0)\\ \mathrm{I}_{n+1}(\kappa_{m,n}r_0)\\ -\mathrm{K}_{n+1}(\kappa_{m,n}r_0)\end{bmatrix}^T$$

Appendix C. Matrices for *n* nodal diameters

$\mathbf{S}_n=\mathrm{diag}\begin{bmatrix}\cdots & \Omega_{m,n}{}^2 & \cdots\end{bmatrix}$ and operator diag[•] stands for diagonal matrix. $\mathbf{S}_n=\mathbf{S}_{-n}$ and $\Omega_{m,n}=\kappa_{m,n}{}^2h\sqrt{E/[12\rho(1-\nu^2)]}$. $\mathbf{I}_1$ is the identity matrix with the size of $\mathbf{S}_n$.

$$\mathbf{L}_n=\begin{bmatrix}\ddots & \vdots & \iddots\\ \cdots & k^n_{m_1,m_2} & \cdots\\ \iddots & \vdots & \ddots\end{bmatrix},\ \mathbf{L}_n=\mathbf{L}_{-n},\ \text{and}\ k^n_{m_1,m_2}=k^n_{m_2,m_1}$$

$$m_1,m_2=0,1,\cdots,N_m$$

$$k^n_{m_1,m_2}=a^2\boldsymbol{c}^{\mathrm{T}}_{m_1,n}\left[\int_b^a\left[\sigma_r\boldsymbol{B}'_n(\kappa_{m_1,n}r)^T\boldsymbol{B}'_n(\kappa_{m_2,n}r)+\sigma_\theta\frac{n^2}{r^2}\boldsymbol{B}_n(\kappa_{m_1,n}r)^T\boldsymbol{B}_n(\kappa_{m_2,n}r)\right]r\,\mathrm{d}r\right]\boldsymbol{c}_{m_2,n}$$

$$\mathbf{H}_{n,k}(r_s)=\begin{bmatrix}\ddots & \vdots & \iddots\\ \cdots & [\boldsymbol{B}_n(\kappa_{m_1,n}r_s)\boldsymbol{c}_{m_1,n}\boldsymbol{B}_k(\kappa_{m_2,k}r_s)\boldsymbol{c}_{m_2,k}] & \cdots\\ \iddots & \vdots & \ddots\end{bmatrix}$$

$$\mathbf{H}^0_{n,k}=\mathbf{H}_{n,k}\big|_{\varphi=\varphi_0}$$

$$\mathbf{H}'_{n,k}=\frac{\partial\mathbf{H}_{n,k}}{\partial r_s}\Big|_{\varphi=\varphi_0}$$

$$=\begin{bmatrix}\ddots & \vdots & \iddots\\ \cdots & \begin{matrix}[\boldsymbol{B}'_n(\kappa_{m_1,n}r_0)\boldsymbol{c}_{m_1,n}\boldsymbol{B}_k(\kappa_{m_2,k}r_0)\boldsymbol{c}_{m_2,k}+\\ \boldsymbol{B}_n(\kappa_{m_1,n}r_0)\boldsymbol{c}_{m_1,n}\boldsymbol{B}'_k(\kappa_{m_2,k}r_0)\boldsymbol{c}_{m_2,k}]\end{matrix} & \cdots\\ \iddots & \vdots & \ddots\end{bmatrix}$$

$$\mathbf{H}''_{n,k}=\frac{\partial^2\mathbf{H}_{n,k}}{\partial r_s{}^2}\Big|_{\varphi=\varphi_0}$$

$$=\begin{bmatrix}\ddots & \vdots & \iddots\\ \cdots & \begin{matrix}[\boldsymbol{B}''_n(\kappa_{m_1,n}r_0)\boldsymbol{c}_{m_1,n}\boldsymbol{B}_k(\kappa_{m_2,k}r_0)\boldsymbol{c}_{m_2,k}+\\ \boldsymbol{B}_n(\kappa_{m_1,n}r_0)\boldsymbol{c}_{m_1,n}\boldsymbol{B}''_k(\kappa_{m_2,k}r_0)\boldsymbol{c}_{m_2,k}+\\ 2\boldsymbol{B}'_n(\kappa_{m_1,n}r_0)\boldsymbol{c}_{m_1,n}\boldsymbol{B}'_k(\kappa_{m_2,k}r_0)\boldsymbol{c}_{m_2,k}]\end{matrix} & \cdots\\ \iddots & \vdots & \ddots\end{bmatrix}.$$

Appendix D. System matrices

$$\mathbf{S}=\mathrm{diag}\begin{bmatrix}\cdots & \mathbf{S}_n & \cdots\end{bmatrix},\quad \mathbf{L}=\mathrm{diag}\begin{bmatrix}\cdots & \mathbf{L}_n & \cdots\end{bmatrix}$$
$$\mathbf{I}=\mathrm{diag}\begin{bmatrix}\cdots & \mathbf{I}_1 & \cdots\end{bmatrix},\quad \mathbf{I}_n=\mathrm{diag}\begin{bmatrix}\cdots & n\mathbf{I}_1 & \cdots\end{bmatrix}$$

$$\mathbf{I}_{n^2}=\mathrm{diag}\begin{bmatrix}\cdots & n^2\mathbf{I}_1 & \cdots\end{bmatrix}$$

$$\mathbf{H}(r_s,\theta_s)=\begin{bmatrix}\ddots & \vdots & \iddots\\ \cdots & \dfrac{e^{i(-n+k)\theta_s}}{2\pi\rho h}\mathbf{H}_{n,k}(r_s) & \cdots\\ \iddots & \vdots & \ddots\end{bmatrix},\ \mathbf{H}^0=\mathbf{H}\big|_{\varphi=\varphi_0}$$

$$\mathbf{H}'=\left.\frac{\partial\mathbf{H}}{\partial\varphi}\right|_{\varphi=\varphi_0}=\begin{bmatrix}\ddots & \vdots & \iddots\\ \cdots & \dfrac{e^{i(-n+k)\theta_0}}{2\pi\rho h}\left[r'_0\mathbf{H}'_{n,k}+i(-n+k)\theta'_0\mathbf{H}^0_{n,k}\right] & \cdots\\ \iddots & \vdots & \ddots\end{bmatrix}$$

$$\mathbf{H}''=\left.\frac{\partial^2\mathbf{H}}{\partial\varphi^2}\right|_{\varphi=\varphi_0}=\begin{bmatrix}\ddots & \vdots & \iddots\\ \cdots & \dfrac{e^{i(-n+k)\theta_0}}{4\pi\rho h}\begin{bmatrix}r'_0{}^2\mathbf{H}''_{n,k}+r''_0\mathbf{H}'_{n,k}-(-n+k)^2\theta'_0{}^2\mathbf{H}^0_{n,k}+\\ i(-n+k)(2r'_0\theta'_0\mathbf{H}'_{n,k}+\theta''_0\mathbf{H}^0_{n,k})\end{bmatrix} & \cdots\\ \iddots & \vdots & \ddots\end{bmatrix}$$

Appendix E. Matrices induced by harmonic balance

$$\mathbf{I}_D=\mathrm{diag}\begin{bmatrix}\cdots & \mathbf{I} & \cdots\end{bmatrix},\quad \mathbf{J}_1=\mathrm{diag}\begin{bmatrix}\cdots & j\mathbf{I} & \cdots\end{bmatrix}$$

$$\mathbf{J}_2=\mathrm{diag}\begin{bmatrix}\cdots & j^2\mathbf{I} & \cdots\end{bmatrix}$$

$$\mathbf{I}_D^n=\mathrm{diag}\begin{bmatrix}\cdots & \mathbf{I}_n & \cdots\end{bmatrix},\ \mathbf{I}_D^{n^2}=\mathrm{diag}\begin{bmatrix}\cdots & \mathbf{I}_{n^2} & \cdots\end{bmatrix}$$

$$\mathbf{K}=\mathrm{diag}\begin{bmatrix}\cdots & \mathbf{S}/\Omega_{0,0}{}^2 & \cdots\end{bmatrix}$$

$$\mathbf{K}_\sigma=\mathrm{diag}\begin{bmatrix}\cdots & \mathbf{L} & \cdots\end{bmatrix}$$

$$\mathbf{Q}^0=\mathrm{diag}\begin{bmatrix}\cdots & \mathbf{H}^0 & \cdots\end{bmatrix},\ \mathbf{Q}'=\mathrm{diag}\begin{bmatrix}\cdots & \mathbf{H}' & \cdots\end{bmatrix}$$

$$\mathbf{Q}''=\mathrm{diag}\begin{bmatrix}\cdots & \mathbf{H}'' & \cdots\end{bmatrix}$$

$$\mathbf{T}_j=\begin{bmatrix}\mathbf{O}_1 & \mathbf{O}_2 & \cdots & \mathbf{O}_j & \mathbf{I} & \mathbf{O} & \cdots & \mathbf{O} & \mathbf{O}\\ \mathbf{O} & \mathbf{O}_1 & \mathbf{O}_2 & \cdots & \mathbf{O}_j & \mathbf{I} & \mathbf{O} & \cdots & \mathbf{O}\\ \ddots & \ddots & \ddots & \ddots & \ddots & \ddots & \ddots & \ddots & \ddots\\ \mathbf{O} & \cdots & \mathbf{O} & \mathbf{O}_1 & \mathbf{O}_2 & \cdots & \mathbf{O}_j & \mathbf{I} & \mathbf{O}\\ \mathbf{O} & \mathbf{O} & \cdots & \mathbf{O} & \mathbf{O}_1 & \mathbf{O}_2 & \cdots & \mathbf{O}_j & \mathbf{I}\\ \mathbf{O} & \mathbf{O} & \mathbf{O} & \cdots & \mathbf{O} & \mathbf{O}_1 & \mathbf{O}_2 & \cdots & \mathbf{O}_j\\ \ddots & \ddots & \ddots & \ddots & \ddots & \ddots & \ddots & \ddots & \ddots\\ \mathbf{O} & \mathbf{O} & \mathbf{O} & \mathbf{O} & \mathbf{O} & \cdots & \mathbf{O} & \mathbf{O}_1 & \mathbf{O}_2\\ \mathbf{O} & \mathbf{O} & \mathbf{O} & \mathbf{O} & \mathbf{O} & \mathbf{O} & \cdots & \mathbf{O} & \mathbf{O}_1\end{bmatrix}$$

$$\mathbf{T}_{-j}=\mathbf{T}_j^T$$

References

[1] W.D. Iwan, K.J. Stahl, Response of an elastic disk with a moving mass system, *Transactions of the ASME Journal of Applied Mechanics* 40 (1973) 445–451.

[2] I.Y. Shen, Response of a stationary, damped, circular plate under a rotating slider bearing system, *Transactions of the ASME Journal of Vibration, Acoustics, Stress, and Reliability in Design* 115 (1993) 65–69.

[3] K. Ono, J.S. Chen, D.B. Bogy, Stability analysis for the head–disk interface in a flexible disk drive, *Transactions of the ASME Journal of Applied Mechanics* 58 (1991) 1005–1014.

[4] J.S. Chen, D.B. Bogy, Effects of load parameters on the natural frequencies and stability of a flexible spinning disk with a stationary load system, *Transactions of the ASME Journal of Applied Mechanics* 59 (1992) 230–235.

[5] J.S. Chen, B.D. Bogy, Natural frequencies and stability of a flexible spinning disk–stationary load system with rigid-body tilting, *Transactions of the ASME Journal of Applied Mechanics* 60 (1993) 470–477.

[6] T.H. Young, C.Y. Lin, Stability of a spinning disk under a stationary oscillating unit, *Journal of Sound and Vibration* 298 (2006) 307–318.

[7] Q.H. Zeng, D.B. Bogy, Numerical simulation of shock response of disk–suspension–slider air bearing systems in hard disk drives, *Microsystem Technologies* 8 (2002) 289–296.

[8] J.E. Mottershead, Vibration and friction-induced instability in discs, *The Shock and Vibration Digest* 30 (1998) 14–31.

[9] S.N. Chan, J.E. Mottershead, M.P. Cartmell, Instabilities at subcritical speeds in discs with rotating frictional follower loads, *Transactions of the ASME Journal of Vibration and Acoustics* 117 (1995) 240–242.

[10] J.E. Mottershead, H.J. Ouyang, M.P. Cartmell, M.I. Friswell, Parametric resonances in an annular disc, with a rotating system of distributed mass and elasticity; and the effects of friction and damping, *Proceedings of Royal Society of London Series A* 453 (1997) 1–19.

[11] H.J. Ouyang, J.E. Mottershead, M.P. Cartmell, M.I. Friswell, Friction-induced parametric resonances in discs: effect of a negative friction–velocity relationship, *Journal of Sound and Vibration* 209 (1998) 251–264.

[12] H.J. Ouyang, J.E. Mottershead, M.P. Cartmell, D.J. Brookfield, Friction-induced vibration of an elastic slider on a vibrating disc, *International Journal of Mechanical Sciences* 41 (1999) 325–336.

[13] H.J. Ouyang, J.E. Mottershead, Unstable travelling waves in the friction-induced vibration of discs, *Journal of Sound and Vibration* 248 (2001) 768–779.

[14] H.J. Ouyang, J.E. Mottershead, Optimal suppression of parametric vibration in discs under rotating frictional loads, *Proceedings of the Institution of Mechanical Engineers, Part C: Journal of Mechanical Engineering Science* 215 (2001) 65–75.
[15] H.J. Ouyang, Moving loads and car disc brake squeal, *Noise and Vibration Worldwide* 34 (2003) 7–15.
[16] H.J. Ouyang, J.E. Mottershead, W. Li, A moving-load model for disc-brake stability analysis, *Transactions of the ASME Journal of Vibration and Acoustics* 125 (2003) 53–58.
[17] H.J. Ouyang, Q. Cao, J.E. Mottershead, T. Treyde, Vibration and squeal of a disc brake: modelling and experimental results, *Proceedings of the Institution of Mechanical Engineers, Part D: Journal of Car Engineering* 217 (2003) 867–875.
[18] Q. Cao, H.J. Ouyang, M.I. Friswell, J.E. Mottershead, Linear eigenvalue analysis of the disc-brake squeal problem, *International Journal for Numerical Methods in Engineering* 61 (2004) 1546–1563.
[19] H.J. Ouyang, J.E. Mottershead, Dynamic instability of an elastic disk under the action of a rotating friction couple, *Transactions of the ASME Journal of Applied Mechanics* 71 (2004) 753–758.
[20] G.N. Weisensel, A.L. Schlack, Annular plate response to circumferentially moving loads with sudden radial position changes, *The International Journal of Analytical and Experimental Modal Analysis* 5 (1990) 239–250.
[21] G.N. Weisensel, A.L. Schlack, Response of annular plates to circumferentially and radially moving loads, *Transactions of the ASME Journal of Applied Mechanics* 60 (1993) 649–661.
[22] S.C. Huang, W.J. Chiou, Modeling and vibration analysis of spinning-disk and moving-head assembly in computer storage systems, *Transactions of the ASME Journal of Vibration and Acoustics* 119 (1997) 185–191.
[23] Y.C. Pei, Q.C. Tan, Parametric instability of flexible disk rotating at periodically varying angular speed, *Meccanica* 44 (2009) 711–720.
[24] K. Takahashi, An approach to investigate the instability of the multiple degree of freedom parametric dynamic systems, *Journal of Sound and Vibration* 78 (1981) 519–529.
[25] O. Turhan, Generalized Bolotin's method for stability limit determination of parametrically excited systems, *Journal of Sound and Vibration* 216 (1998) 851–863.
[26] O. Turhan, K. Koser, Parametric stability of continuous shafts, connected to mechanisms with position-dependent inertia, *Journal of Sound and Vibration* 277 (2004) 223–238.
[27] O. Turhan, G. Bulut, Dynamic stability of rotating blades (beams) eccentrically clamped to a shaft with fluctuating speed, *Journal of Sound and Vibration* 280 (2005) 945–964.